ACS APPLIED MATERIALS & INTERFACES

www.acsami.org

Research Article

Mechano-Responsive, Tough, and Antibacterial Zwitterionic Hydrogels with Controllable Drug Release for Wound Healing Applications

Kun Fang, Rong Wang,* Hua Zhang, Linjie Zhou, Ting Xu, Ying Xiao, Yang Zhou, Guorong Gao, Jing Chen, Donglei Liu,* Fanrong Ai, and Jun Fu*

Cite This: *ACS Appl. Mater. Interfaces* 2020, 12, 52307−52318

Read Online

ACCESS | Metrics & More | Article Recommendations | Supporting Information

ABSTRACT: Acute wounds subject to frequent deformations are difficult to be treated because the healing process was easily interfered by external mechanical forces. Traditional wound dressings have limited efficacy because of their poor mechanical properties and skin adhesiveness and difficulty in the delivery of therapeutic drugs effectively. As such, tough and skin-adhesive wound dressings with sustainable and stimuli-responsive drug release properties for treatment of those wounds are highly desirable. For this purpose, we have developed a mechano-responsive poly(sulfobetaine methacrylate) hydrogel which aims to control the delivery of antibiotic drug upon application of mechanical forces. Diacrylated Pluronic F127 micelles were used as a macro-cross-linker of the hydrogel and loaded with hydrophobic antimicrobial drugs. The micelle-cross-linked hydrogel has excellent mechanical properties, with the ultimate tensile strength and tensile strain of up to 112 kPa and 1420%, respectively, and compressive stress of up to 1.41 MPa. Adhesiveness of the hydrogel to the skin tissue was ~6 kPa, and it did not decrease significantly after repetitive adhesion cycles. Protein adsorption on the hydrogel was significantly inhibited compared to that on commercial wound dressings. Because of the mechano-responsive deformation of micelles, the release of drug from the hydrogel could be precisely controlled by the extent and cycles of mechanical loading and unloading, endowing the hydrogel with superior antibacterial property against both Gram-positive and Gram-negative bacteria. In addition, drug penetration into the skin tissue was enhanced by mechanical stress applied to the hydrogel. The micelle-cross-linked zwitterionic hydrogel also showed good cell biocompatibility, negligible skin irritation, and healing capacity to acute skin wounds in mice. Such a tough mechano-responsive hydrogel holds great promise as wound dressings for acute wounds subjected to frequent movements.

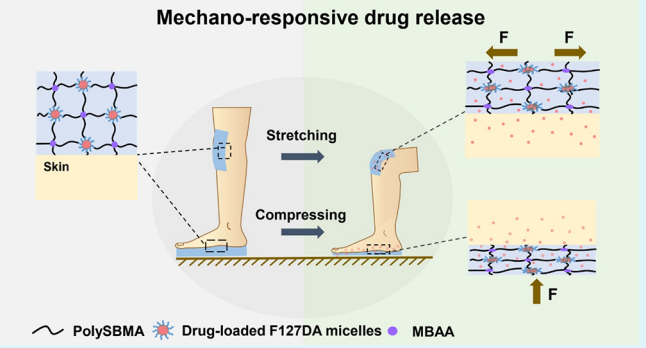

KEYWORDS: *mechano-responsive, antibacterial, tough hydrogels, antifouling, drug release*

1. INTRODUCTION

Treatment of acute cutaneous wounds has attracted tremendous attention globally in recent decades.[1−3] Compared to traditional wound dressings such as medical gauze and bandage, hydrogels shed light on wound management, attributed to their good biocompatibility and capability to promote healing in a moisture environment.[4] More importantly, hydrogels can serve as a carrier to deliver therapeutic drugs for preventing wound infection and promoting the healing process.[5−7] However, most of the research works on hydrogel dressings have been focusing on treatment of wounds in a static environment. In fact, wounds on moving body parts are usually subjected to various mechanical forces. For example, wounds on the elbow, knee, and ankle are subjected to stretching forces due to body movement, while those underfoot are subjected to compressive forces when standing or walking. Under such dynamic circumstances, most of the traditional hydrogels are not capable of preventing mechanical rupture, maintaining their functionality, nor fitting in compliance with the skin. As a result, the healing process in those wounds is prone to be interfered or delayed, resulting in bleeding, pain, or even severe infections. Considering the inherent dynamic mechanical environment at these wound sites, development of a tough adhesive hydrogel dressing which delivers therapeutic drugs in response to body movement is of

Received: July 19, 2020
Accepted: November 2, 2020
Published: November 12, 2020

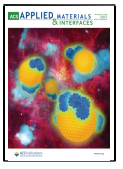

https://dx.doi.org/10.1021/acsami.0c13009
ACS Appl. Mater. Interfaces 2020, 12, 52307−52318

great clinical importance.[8,9] Various mechano-responsive hydrogels that adapt their properties to external mechanical stimuli have been developed recently.[10] Among these, control of drug delivery from mechano-responsive hydrogels is especially important for wound treatment applications.[11] In addition, an ideal wound dressing material should be tissue adhesive, antibacterial, and biocompatible.

Block copolymer micelles are excellent candidates as nanocarriers for loading and delivery of therapeutic drugs because of the hydrophobic association between its micelle core and drug molecule.[12−14] For example, hydrophobic antimicrobial 4-amide-piperidine-C12 (4AP12) has been incorporated in Pluronic F127 diacrylate (F127DA) micelles, which were graft-copolymerized with acrylic acid as a hydrogel coating for catheter modification.[15] A sustained release of the antimicrobial 4AP12 from the hydrogel coating to inhibit bacterial colonization over at least 14 days was achieved. On the other hand, functional block copolymer micelles can be used as macro-cross-linkers to synthesize hydrogels with outstanding mechanical properties.[16−18] For example, F127DA micelles can be used as a macro-cross-linker and serve as an energy dissipator, endowing the poly(acrylamide-*co*-acrylic acid) hydrogel with outstanding tensile strength, toughness, and self-recovery properties.[19] The polymer chains or the micelles in the hydrogel deformed upon application of external mechanical forces, resulting in a reduction in the strength of hydrophobic interaction in the micelle core. However, there is still lack of studies on utilizing the mechano-responsive property of micelles in hydrogels to control drug release in a precise manner for wound healing applications.

Zwitterionic polymers such as poly(sulfobetaine methacrylate) (polySBMA) have widely been used as antifouling materials, which form a hydration layer on the surface because of the solvation of zwitterionic groups.[20,21] The polySBMA hydrogel also exhibits excellent adhesiveness to skin tissues, attributed to the ion−dipole and dipole−dipole interactions between the zwitterionic groups of polySBMA and functional groups on the skin surface.[22] In addition, it has been reported that polySBMA hydrogels facilitate the wound healing process by enhancing cell migration and proliferation and autolytic debridement,[23] and thereby promote angiogenesis and granulation tissue formation.[24]

In this study, a tough, antifouling, and antibacterial hydrogel which delivered bioactive drugs in a mechano-responsive manner has been developed, which aims to address the problem in healing cutaneous wounds in a dynamic mechanical environment. F127DA micelles served as macro-cross-linkers and drug carriers, while zwitterionic polySBMA endowed the hydrogel with tissue adhesiveness and antifouling property. The release of drug from the hydrogel could be precisely controlled by stretching or compressing the hydrogel. The mechanical properties, tissue adhesiveness, protein adsorption, antibiofilm formation properties, cytotoxicity, skin irritation, and *in vivo* wound healing performance of the hydrogel were studied and optimized. More importantly, the drug release profile of the hydrogel under the stimulation of various mechanical strains as well as drug penetration in the skin tissue was investigated.

2. EXPERIMENTAL SECTION

2.1. Materials. Rifampicin (97%), erythromycin (titer ≥850 μg/mg), indomethacin (99%), [2-(methacryloyloxy)ethyl]dimethyl-(3-sulfopropyl)ammonium hydroxide (SBMA, 97%), *N*,*N*′-methylenebis(acrylamide) (MBAA, 99%), ammonium persulfate (APS, 98%), *N*,*N*,*N*′,*N*′-tetramethylethylenediamine (TEMED, 99%), bovine serum albumin (BSA, 96%), and agar were purchased from Aladdin Chemistry Co., Ltd. Tryptic soy broth and lysogeny broth were purchased from Hangzhou Baisi Biotechnology Co., Ltd. Bradford Reagent (catalog number: B6916) and Pluronic F127 (MW = 12,600 Da) were purchased from Sigma-Aldrich (Shanghai, China). *N*-Butyl-4-(2-aminoethylamino)-1,8-naphthalimide was purchased from Shanghai Jinjinle Industry Co., Ltd. *Staphylococcus aureus* (*S. aureus*) 5622, *Staphylococcus epidermidis* (*S. epidermidis*) 5823, and *Escherichia coli* (*E. coli*) 5621 were gifts from the Affiliated Hospital of School of Medicine of Ningbo University. The strains were isolated from patients with cutaneous wound infections. The minimum inhibitory concentrations (MICs) of rifampicin for *S. aureus*, *S. epidermidis*, and *E. coli* were 0.008, 0.063, and 16 μg/mL, respectively. Rabbit bone marrow mesenchymal stem cells (BMSCs) were a gift from Ningbo University.

2.2. Preparation of Drug-Loaded Micelles. Pluronic F127DA was prepared by acrylation of Pluronic F127, as described in a previous work.[25] Drug-loaded F127DA micellar dispersion was prepared by the thin-film hydration method, as described in our previous work.[15] Briefly, specific amounts of rifampicin and F127DA were dissolved in 5 mL of methylene chloride under stirring. The organic solvent was then removed by vacuum drying, and the compound was dissolved using 5 mL of deionized water with continuous stirring at room temperature to obtain a transparent and clean drug-loaded micellar dispersion. The hydrodynamic size of F127DA micelles, rifampicin-loaded F127DA micelles, and rifampicin aggregates in aqueous dispersion was measured by dynamic light scattering (DLS) using a Zetasizer Nano ZS (Malvern, UK). The rifampicin-loaded micelle dispersion was filtered using a 0.22 μm filter to remove any rifampicin aggregates, and the absorbances of solution at 335 nm before and after filtration were measured using a UV spectrophotometer (TU-1810, Persee, China).[26] The drug amount was determined by the measurement of UV absorbance at 335 nm of the dispersion after filtration. The loading efficiency (E) was calculated using eq 1

$$E = \frac{A_2}{A_1} \times 100\% \quad (1)$$

where A_1 and A_2 are the absorbances of dispersion before and after filtration, respectively.

2.3. Hydrogel Preparation. The drug-loaded micellar dispersion was mixed with a certain amount of SBMA with continuous stirring until it dissolved fully. Specific amounts of MBAA, APS, and TEMED were subsequently dissolved in the solution to obtain the hydrogel precursor. The precursor solution was injected into a closed glass mold and incubated at 37 °C overnight to form a hydrogel. The compositions used for the preparation of hydrogels are shown in Table S1. The hydrogels were denoted F_xS_yR, where F refers to F127DA, x refers to the concentration of F127DA in mmol/L, S refers to SBMA, y refers to the concentration of SBMA in mol/L, and R refers to rifampicin. Hydrogels loaded with erythromycin, indomethacin, or fluorescein [*N*-butyl-4-(2-aminoethylamino)-1,8-naphthalimide] were prepared in a similar manner as described above.

The prepared hydrogel was frozen in liquid nitrogen, fractured to obtain a cross section, and freeze-dried. The hydrogel sample was then coated with platinum, and the cross section was observed using a scanning electron microscope (S4800, Hitachi, Japan).

2.4. Swelling Ratio and Degradation of Hydrogels. For the swelling test, hydrogels were cut into cylindrical shape (9 mm in diameter and 1 mm in thickness) and soaked in 15 mL of deionized water or NaCl solutions with different concentrations (0.15, 0.5, 1, and 2 mol/L) at room temperature for 24 h. The weights of the hydrogel disks before and after swelling were recorded. The swelling ratio (Q) of each sample was calculated using eq 2

https://dx.doi.org/10.1021/acsami.0c13009
ACS Appl. Mater. Interfaces 2020, 12, 52307−52318

$$Q = \frac{W_2 - W_1}{W_1} \times 100\% \quad (2)$$

where W_1 and W_2 are the weight (in gram) of hydrogel samples before and after swelling, respectively.

For the degradation test, the hydrogel sample (9 mm in diameter and 1 mm in thickness) was immersed in 15 mL of phosphate-buffered saline (PBS, 10 mM, pH 7.2 ± 0.2) at 37 °C. At each fixed time point, water on the hydrogel surface was removed using a filter paper and the sample was weighed. The weight loss (W_L) of the hydrogel was calculated using eq 3

$$W_L = \frac{W_a - W_b}{W_a} \times 100\% \quad (3)$$

where W_a and W_b are the weight (in gram) of hydrogel samples before and after the degradation test, respectively.

2.5. Mechanical Properties. Hydrogels were cut into 40 mm × 10 mm × 1 mm size and their tensile properties were tested with a universal testing machine (CMT-1104, SUST, China) at a crosshead speed of 100 mm/min until breaking point. At least three hydrogel samples were tested for each group. The Young's modulus of the hydrogel was determined from the slope of the stress−strain curve within a strain range from 0 to 10%. For the cyclic tensile test, the hydrogel samples were coated with silicone oil to avoid water loss and tested under the same conditions as described above with a maximum strain of 100%. For the compression test, hydrogel samples were cut into a cylindrical shape (15 mm in diameter and 2 mm in thickness) and compressed at a crosshead speed of 10% strain per minute at room temperature using the universal testing machine.

2.6. *Ex Vivo* Tissue Adhesion. The lap shear method was carried out to evaluate the adhesive strength of hydrogels to porcine skin (obtained from a nearby supermarket). Prior to the test, the fresh porcine skin was rinsed with copious amounts of deionized water to remove any dirt on it. Hydrogels were cut into 15 mm × 15 mm × 1 mm size and sandwiched between two pieces of porcine skin (40 mm × 15 mm × 3 mm) (Figure S1). To ensure the compatibility of the hydrogel with the skin surface, a 100 g weight was placed on top of the hydrogel−porcine skin assembly for 5 min before testing. The two ends of the assembly were fixed on a universal testing machine by clamps, and the assembly was pulled at a shear rate of 50 mm/min until the breaking point. At least three samples for each group were tested. The adhesion strength was calculated by dividing the fracture adhesion force by the contact area between the hydrogel and the porcine skin (225 mm^2).

2.7. Protein Adsorption. Hydrogels, UrgoTul Ag dressing (URGO Laboratories, Chenôve, France), and chitin dressing (Renhe Medical Supplies Industry and Trade Co., Ltd., Zhejiang, China) were cut into cylindrical shape (9 mm in diameter and 1 mm in thickness). All samples were soaked in 2 mL PBS for 1 h to achieve the swelling equilibrium state prior to the test. After gently removing the PBS solution, each sample was immersed in 2 mL BSA solution (1 mg/mL in PBS) for 4 h at room temperature. The sample was then taken out, and the concentration of the remaining BSA solution was determined using the Bradford method with a slight modification.[27] Briefly, 100 μL of the collected BSA solution was added to 3 mL of Bradford Reagent and vortexed gently for thorough mixing. After 10 min of reaction, the absorbance of the protein−dye complex at 595 nm was measured with a UV spectrophotometer. The standard calibration curve was obtained following the manufacturer's protocol. The concentration of protein in the remaining solution was calculated from the standard calibration curve. The amount of protein adsorbed on the hydrogel sample was calculated by subtracting the remaining amount from the initial amount of BSA in the solution.

2.8. Biofilm Formation Assay. *S. aureus* and *S. epidermidis* were cultured in tryptic soy broth and *E. coli* was cultured in lysogeny broth at 37 °C for 18 h under shaking, then diluted using fresh culture broth 1000 times before use. Hydrogels, UrgoClean (URGO Laboratories, Chenôve, France), and UrgoTul Ag dressings were cut into cylindrical shape (9 mm in diameter and 1 mm in thickness) and placed in a 24-well plate. Two mL of bacterial suspension was added into each well. The plate with samples was incubated statically at 37 °C for 24 h. After incubation, the bacterial suspension was removed and the samples were gently rinsed with PBS three times to wash away any nonadherent or loosely adhered bacteria. The sample was then used for SEM qualitative analysis or bacteria quantification test. For SEM analysis, bacteria adhering to samples were fixed by incubating the samples in 2.5% glutaraldehyde for 4 h at room temperature. Each sample was then serially dehydrated with 25, 50, 75, and 100% ethanol for 15 min in each step. The samples were dried under vacuum for 24 h and then coated with platinum for SEM analysis. For the quantification test, the samples were placed in a centrifuge tube containing 4 mL PBS. The tubes with the samples were ultrasonicated for 7 min and vortexed for 30 s to release bacteria into PBS solution. After serial dilution, the bacterial suspension was spread on appropriate agar plates (tryptic soy agar for *S. aureus* and *S. epidermidis* and lysogeny agar for *E. coli*) and cultured overnight at 37 °C to calculate the number of viable bacteria.

2.9. Drug Release upon Hydrogel Stretching. Hydrogels were cut into strips of 60 mm × 25 mm × 2 mm size, and both ends of the hydrogel strip (10 mm in length) were covered by silicone rubber and fixed with binder clips. The assembly was immersed in a container with 10 mL deionized water (Figure S2). The exposed surface area of the hydrogel to water was approximately 21.6 cm^2 in its initial status. The hydrogel strip was stretched by a determined strain (60 or 80%) and then released to the initial status at a constant speed of 6 s/cycle (Video S1). The control experiment was carried out by incubating the same assembly of hydrogel strip−silicone rubber−binder clips in deionized water without stretching. After every 50 tensile cycles (or 300 s for control groups), 4 mL of solution containing any released drug was collected and replaced by 4 mL fresh deionized water. The absorbance of the solution at 335 nm was measured to determine the concentration of released rifampicin. The cumulative amount of drug released from hydrogels under different tensile strains was calculated by summing up the amount of drug released after every 50 tensile cycles or 300 s.

2.10. Drug Release upon Hydrogel Compression. Hydrogel disks (15 mm in diameter and 2 mm in thickness) were placed in a container with 6 mL deionized water. An acrylic assembly fixed by clamps was used to compress samples in a universal testing machine (Figure S3). As the upper surface of hydrogel was covered by the acrylic assembly and the lower surface adhered to the plastic container, the exposed surface area of hydrogel to water was approximately 0.94 cm^2 in its initial status. Hydrogel disks were compressed by 40, 50, or 60% of their initial thickness and then released to their initial states at a constant speed of 6 s/cycle (Video S2). The control experiment was carried out by incubating a hydrogel sample of the same size in 6 mL deionized water with the acrylic assembly placed on the top but without compression. Four mL solution was collected and replaced with the same amount of fresh deionized water every 40 cycles (or 240 s for control groups). The cumulative amount of drug released was measured in the same manner as described above.

2.11. *In Situ* Small-Angle X-ray Scattering of Hydrogels. *In situ* small-angle X-ray scattering (SAXS) analysis of hydrogels under stretching or compressing forces was conducted using a Xenocs GeniX 3D Cu ULD microbeam X-ray generator and the wavelength of the X-rays was fixed at 0.154 nm. A hydrogel strip of 40 mm × 10 mm × 2 mm size was fixed to a tensile stage module. The distance from the sample to the MAR345 X-ray detector (marXperts, Norderstedt, Germany) was 2554 mm. The 2D scattering images of the hydrogel at its initial length and when stretched by 80% were obtained with an acquisition time of 1800 s. For the SAXS analysis of hydrogels under compressive strain, the hydrogel disk (9 mm in diameter and 3 mm in thickness) was sandwiched between two polyimide films, and the 2D scattering images of the hydrogel with its original thickness as well as when compressed by 60% were recorded with an acquisition time of 1800 s.

2.12. Antibacterial Tests. The antibacterial property of the solutions containing drugs released from hydrogels after stretching or compressing was evaluated by the disk diffusion method using *S.*

https://dx.doi.org/10.1021/acsami.0c13009
ACS Appl. Mater. Interfaces 2020, 12, 52307−52318

Scheme 1. Schematic Diagram Illustration of (a) Preparation of Drug-Loaded F127DA Micelle, (b) Preparation of F_xS_yR Hydrogels, and (c) Deformation of Hydrogel Network and Drug Release under Mechanical Force

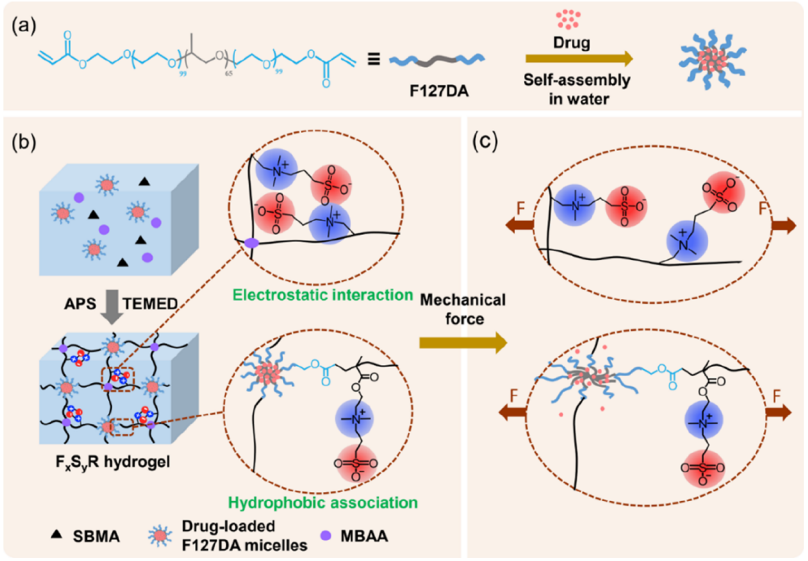

aureus, *S. epidermidis*, and *E. coli*. Briefly, an overnight-cultured bacterial suspension was diluted using culture medium by 1000 times. One hundred microliters of bacterial suspension was spread on the appropriate agar plate (tryptic soy agar for *S. aureus* and *S. epidermidis* and lysogeny agar for *E. coli*). Sterilized filter paper disks (6 mm in diameter) were placed on the agar plate. Ten microliters of the drug solution obtained from the release experiment described above was then applied to the filter paper disk. After incubation at 37 °C for 18 h, the diameter of inhibitory zone around the paper disk on the agar plate was recorded.

2.13. *Ex Vivo* Drug Penetration Evaluation. Fresh porcine tissues were cut into bulks (50 mm × 40 mm; 15 and 3 mm thick for fluorescence imaging and antibacterial test, respectively), carefully rinsed with copious amounts of deionized water to remove any dirt, and assembled with the hydrogel (20 mm in diameter and 10 mm in thickness and loaded with fluorescein or rifampicin) and a filter paper in a universal testing machine (Figure S4). The whole assembly was compressed by 60% strain and then released, which are repeated for 1000 cycles with a speed of 6 s/cycle using a universal testing machine (Video S3). The same hydrogel−tissue−filter paper assembly without compression placed at room temperature for the same duration (i.e., 100 min) served as control. The porcine tissue was cut vertically to obtain a cross section, which was observed using a confocal laser scanning microscope (TCS SP5, Leica, Germany) to characterize the penetration of fluorescent molecules into the porcine tissue after cyclic compression. The fluorescence intensity curve was obtained by image analysis using ImageJ (version 1.52p). The disk diffusion test was conducted to evaluate if any antibiotic has penetrated through the pig tissue and collected by the filter paper after the cyclic compression.

2.14. *In Vitro* Cytotoxicity Assay. The cytotoxicity test of hydrogels was conducted using rabbit BMSCs according to the standard protocol stated in ISO 10993-5:2009.[28] Briefly, 100 mg of $F_6S_{4.0}$ or $F_6S_{4.0}R$ hydrogel was incubated in 5 mL of Dulbecco's modified Eagle's medium (DMEM, Hyclone, supplemented with 10% fetal bovine serum, 1.0 × 10^5 U/L penicillin, and 100 mg/L streptomycin) at 37 °C for 24 h to obtain the extract solution. The $F_6S_{4.0}R$ hydrogel was also stretched by 80% strain for 250 cycles in DMEM under similar releasing conditions as described above. The extract medium containing released drugs was then filtered using a 0.22 μm sterile filter. Rabbit BMSCs were seeded in a 96-well plate with the density of 10^4 cells per well and incubated for 24 h to achieve a monolayer culture. After that, the culture medium was replaced by the extract solution of hydrogels. Fresh culture medium was used as control. After cultured for 36 h, the cell counting kit-8 (CCK-8) (TransGen Biotech Co., Ltd., China) assay was conducted to evaluate the BMSC viability according to the manufacturer's protocol. The absorbance at 450 nm of medium in each well was measured using a microplate reader (SpectraMax 190, Molecular Devices, United States). The cell viability was calculated as the percentage of absorbance value of the experimental group relative to that of the control group. To determine the cytotoxicity effect of rifampicin, DMEM containing 1, 2, 4, and 16 μg/mL rifampicin was used to culture the cells, and the cell viability was evaluated using the CCK-8 assay.

2.15. *In Vivo* Skin Irritation Test and Wound Healing Evaluation. Institute of cancer research male mice (25−30 g) were housed in the Animal Center of Ningbo University. All animals had free access to standard food and water. Hair on the mouse back was shaved after anesthesia. All mice were euthanized peacefully after experiments. All procedures for animal experiments were approved by the Institutional Animal Ethics Committee of Ningbo University.

The skin irritation test was conducted according to ISO 10993-10.[29] The $F_6S_{4.0}R$ hydrogel (8 mm in diameter and 1 mm in thickness) was placed on the back skin of the animal and a medical gauze (wetted with PBS) of same size was used as control. The hydrogel and the gauze were fixed using a Tegaderm dressing (3M, Minnesota, United States). The appearance of the treated site was photographed after 1, 24, 48, and 72 h. The irritation score was given according to the standard protocol. At least three mice were used for each group.

A full-thickness skin defect mice model was used to evaluate the *in vivo* wound healing performance of the $F_6S_{4.0}R$ hydrogel. Briefly, two defect sites of 8 mm diameter were created on the back skin of the mouse. One of the defect sites was placed with the $F_6S_{4.0}R$ hydrogel (8 mm in diameter and 1 mm in thickness) and the other one was left without any treatment as control. The wounded site was covered with a 3M Tegaderm dressing. On days 0, 2, 5, 7, and 14, the appearance of the wound site was photographed, and the size of the wound was measured using ImageJ (version 1.52p). At least three mice were used for each group.

Tissue slices of 5 μm thickness from the treated/wound site were obtained by paraffin section. Histological evaluation was conducted by hematoxylin and eosin (H&E, Solarbio G1120, China) staining, followed by microscope observation (DFC450 C, Leica, Germany).

2.16. Statistical Analysis. All results presented were averaged from at least three samples for each group. Student's *t*-test was applied to determine the statistical significance between various groups. A p value of <0.05 was considered to be statistically significant.

https://dx.doi.org/10.1021/acsami.0c13009
ACS Appl. Mater. Interfaces 2020, 12, 52307−52318

3. RESULTS AND DISCUSSION

3.1. Preparation of Drug-Loaded F127DA Micelles. F127DA was synthesized by acrylation of Pluronic F127, as described in our previous work.[25,30] The degree of substitution of acryloyl groups was about 98.7%, as measured by peak integration of the ^{1}H NMR spectrum (Figure S5). F127DA, as an amphiphilic vinyl-terminated triblock copolymer, can self-assemble into micelles in an aqueous environment.[31] The F127DA micelles can be used as efficient nanoscaled drug carriers for encapsulation of therapeutic drugs.[17,32,33] A hydrophobic antibiotic, rifampicin, was chosen as a model drug and loaded in F127DA micelles because of the hydrophobic association between the drug molecules and the hydrophobic polypropylene oxide segment of F127DA (Scheme 1a). To investigate the maximum drug-loading capacity of F127DA micelles, different amounts of rifampicin were incubated with F127DA in deionized water. The hydrodynamic size of F127DA micelles without drug was about 35 nm (Figure S6a). The micellar size slightly decreased with increasing molar ratio of rifampicin to F127DA from 0.5:6 to 1.5:6, probably due to enhancement of hydrophobic association between the hydrophobic core and drug molecules (Figure S6b–d). Large micrometer-sized aggregates were observed when the molar ratio of rifampicin to F127DA further increased to 4.5:6, indicating that F127DA micelles were not able to encapsulate more drug molecules above this concentration (Figure S6d). Without F127DA, the hydrophobic rifampicin molecules form large aggregates in deionized water (Figure S6e). The rifampicin-loaded F127DA micellar dispersions were filtered using a 0.22 μm filter to remove any aggregates of the drug not encapsulated in micelles. The loading efficiency of $F_6R_{0.5}$, $F_6R_{1.5}$, and $F_6R_{4.5}$ dispersions (the feeding molar ratio of rifampicin to F127DA was 0.5:6, 1.5:6, and 4.5:6, respectively) was thus determined to be 99.5, 99.6, and 88.0%, respectively (Figure S7). Therefore, the optimal molar ratio of 1.5:6 of rifampicin to F127DA was used to prepare rifampicin-loaded micelles and hydrogels in the rest of this study.

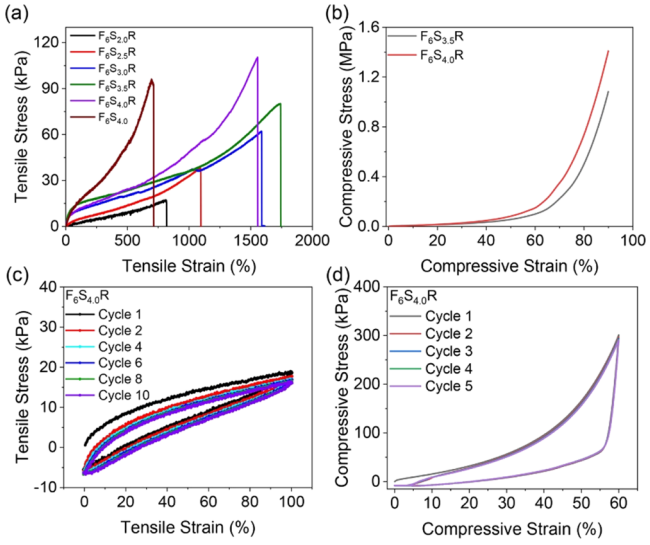

Figure 1. Mechanical properties of F_xS_yR hydrogels. (a) Representative tensile stress–strain curves of hydrogels with different polySBMA contents. (b) Representative compressive stress–strain curves of hydrogels with different polySBMA contents. (c) Cyclic tensile stress–strain curve and (d) cyclic compressive stress–strain curve of the $F_6S_{4.0}R$ hydrogel.

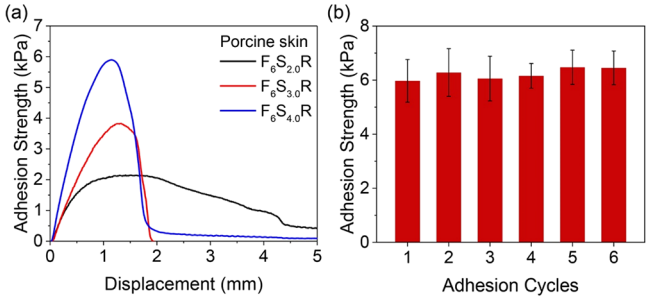

Figure 2. (a) Adhesion strength–displacement curve of hydrogels against the porcine skin. (b) Cyclic adhesion strength of $F_6S_{4.0}R$ hydrogels against the porcine skin.

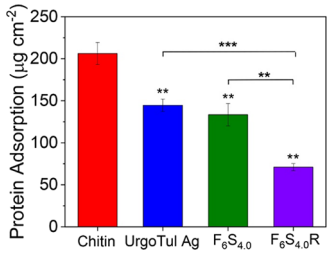

Figure 3. Protein adsorption on chitin and UrgoTul Ag dressings and on $F_6S_{4.0}$ and $F_6S_{4.0}R$ hydrogels after incubation in 1 mg/mL BSA solution for 4 h. ** and *** denote statistically significant difference with $p < 0.01$ and $p < 0.001$ in comparison with the chitin dressing or between two groups, respectively.

3.2. Hydrogel Preparation and Its Mechanical Properties. Acute wounds on joints such as fingers, wrists, elbows, knees, and feet are difficult to be treated, because of the various mechanical forces and frequent skin deformation on these sites. Therefore, it is highly desirable to have dressings with appropriate mechanical properties and stability for treatment of wounds on these dynamic sites. In this study, a tough hydrogel with mechano-responsive release of drugs was designed and prepared by free radical polymerization of SBMA, with drug-loaded F127DA micelle and MBAA as the macro-cross-linker and chemical cross-linker, respectively (Scheme 1b,c).

The as-prepared hydrogel had high stretchability and compressive property (Figure 1). With the concentration of SBMA in the precursor solution increasing from 2 to 4 mol/L, the ultimate tensile strength of the hydrogel increased remarkably from 11 to 112 kPa (Figures 1a, S8a). The average fracture tensile strain of hydrogels with 3.5 and 4 mol/L of SBMA was 1637 and 1420%, respectively (p-value: 0.37, Figure S8a). The Young's modulus increased from 3.35 to 44.40 kPa when the SBMA concentration increased from 2 to 4 mol/L (Figure S8b), which is close to that of the human skin (1–10 kPa).[34] The hydrogels also showed high ultimate compressive strength of 1.09 and 1.41 MPa for $F_6S_{3.5}R$ and $F_6S_{4.0}R$ hydrogels, respectively (Figure 1b). Hysteresis loops were observed in all cyclic tensile loading/unloading cycles of $F_6S_{4.0}R$ hydrogel (Figure 1c), which means that energy dissipation happened during the loading/unloading process. After the first tensile cycle, the hysteresis loop became smaller and almost overlapped with the consecutive loops, indicating that there was permanent destruction of some covalent bonds in the first tensile cycle, and the hydrogel can recover quickly

https://dx.doi.org/10.1021/acsami.0c13009
ACS Appl. Mater. Interfaces 2020, 12, 52307–52318

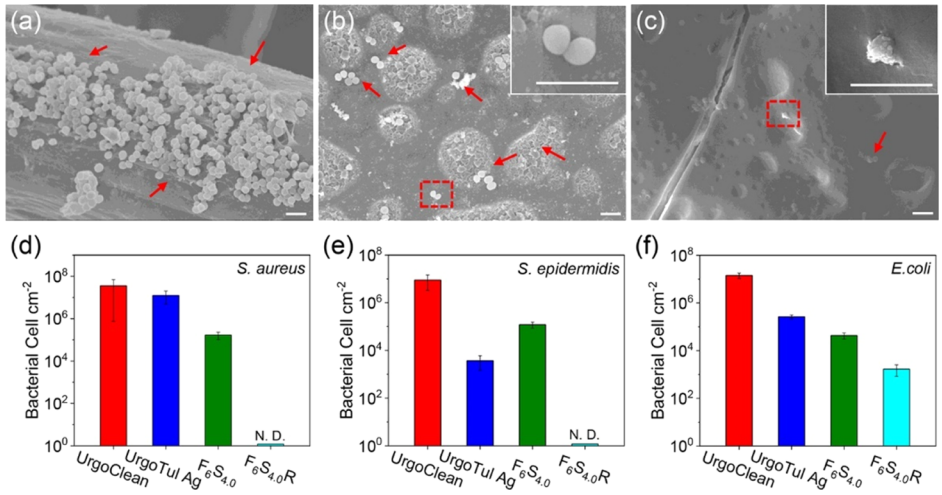

Figure 4. SEM images of *S. aureus* biofilm formation on (a) UrgoClean, (b) $F_6S_{4.0}$ hydrogel, and (c) $F_6S_{4.0}R$ hydrogel. Red arrows indicate the adherent *S. aureus* bacteria on the surface of materials. Scale bars represent 2 μm. Quantification of viable adherent (d) *S. aureus*, (e) *S. epidermidis*, and (f) *E. coli* on UrgoClean, UrgoTul Ag, $F_6S_{4.0}$, and $F_6S_{4.0}R$ hydrogels after incubation in culture broth (initial inoculum was 10^5 cells/mL) for 24 h. N. D. denotes not detected.

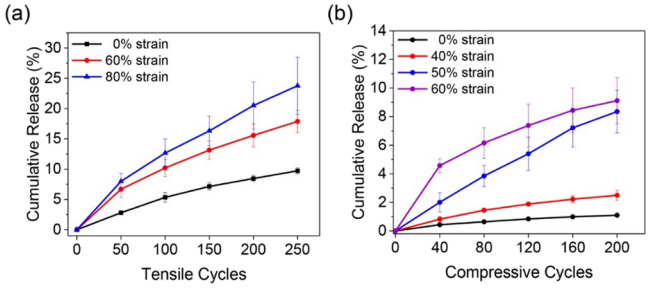

Figure 5. Drug release from the $F_6S_{4.0}R$ hydrogel under different (a) tensile strains and (b) compressive strains.

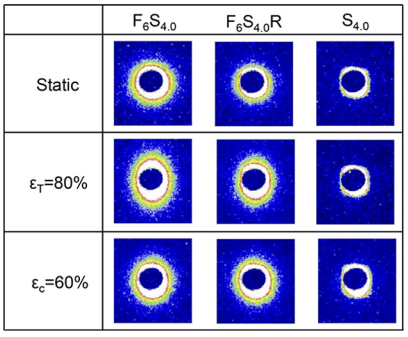

Figure 6. SAXS images of $S_{4.0}$, $F_6S_{4.0}$ and $F_6S_{4.0}R$ hydrogels under static, stretched, and compressed conditions, respectively.

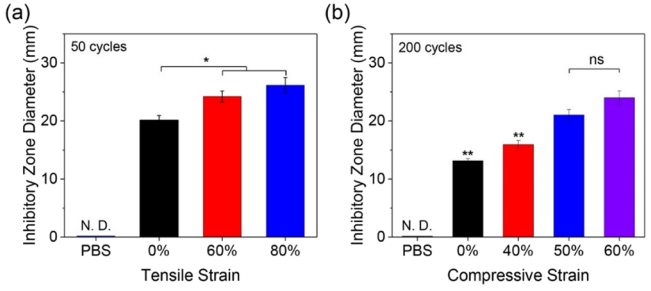

Figure 7. Inhibitory zone diameters of different drug release solutions against *S. aureus*. The drug release solutions were collected after the $F_6S_{4.0}R$ hydrogel was subjected to different degrees of (a) stretching for 50 cycles, and (b) compressing for 200 cycles. * and ** denote statistically significant difference with $p < 0.05$ and $p < 0.01$, respectively, in comparison with the control group and other experimental groups. N. D. denotes not detected. ns denotes no significance.

from deformation. Overlapped hysteresis loops during the compressive loading/unloading process (Figure 1d) demonstrated that the hydrogel can recover after certain conformational deformation.

As there is a large amount of zwitterionic groups in the polySBMA chains of hydrogels, the electrostatic interaction between positive- and negative-charged groups is likely to serve as intra- and inter-chain physical cross-linking, contributing to the high mechanical properties of hydrogels. The swelling ratio of the $F_6S_{4.0}$ hydrogel in NaCl solution was 944%, which was nearly 10 times higher than that in deionized water (96%) (Figure S9a). This is because the electrostatic interaction within zwitterionic groups was shielded by Na^+ and Cl^- ions, resulting in decreased attractive forces between polymer chains, which is known as the antipolyelectrolyte effect of zwitterionic polymers.[35] In addition, NaCl solution of 1 or 2 mol/L instead of water was used to prepare the precursor solution to shield the electrostatic interaction of polySBMA chains in the as-prepared hydrogel. The fracture strength of the $F_6S_{4.0}$−NaCl hydrogel decreased significantly from 67.37 to 52.16 kPa and the fracture strain decreased from 532.20 to 503.97% with the increase of NaCl concentration from 1 to 2 mol/L (Figure S9b,c). It was thus verified that the electrostatic interaction serves as an energy dissipator in the hydrogel network upon mechanical forces, conferring the hydrogel with high mechanical properties.

Incorporation of drug-loaded F127DA micelles also affected the mechanical properties of the hydrogel. With increase of the drug-loaded micelles from 3 to 6 mmol/L, the ultimate tensile strength of the hydrogel increased from 48 to 138 kPa. However, it decreased to 111 kPa as the concentration of drug-loaded F127DA micelles was further increased to 12 mmol/L (Figure S9d). The fracture tensile strain of hydrogels also showed a similar trend with the increase of drug-loaded F127DA micelles. This is because with the drug-loaded

https://dx.doi.org/10.1021/acsami.0c13009
ACS Appl. Mater. Interfaces 2020, 12, 52307−52318

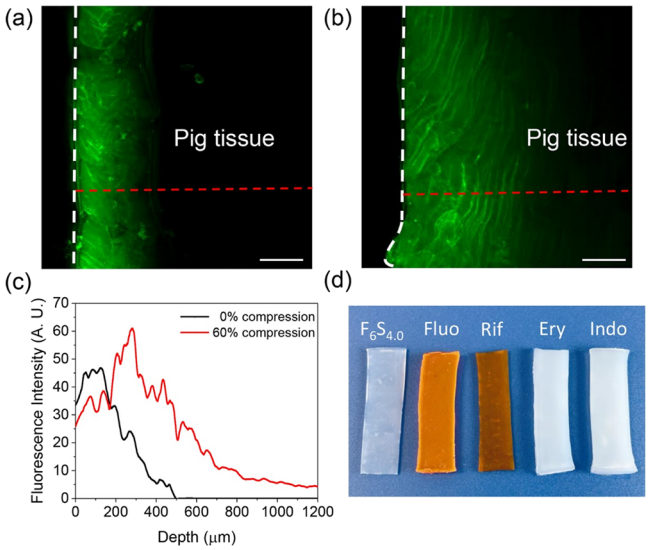

Figure 8. Confocal fluorescence images of the cross section of porcine tissue after fluorescein penetration (a) without compression and (b) with 60% compression for 1000 cycles. Scale bars represent 250 μm. The red dotted line indicates the measurement area of fluorescence intensity. (c) Plot of the penetration depth of fluorescein into the porcine tissue from the hydrogel with or without compression. (d) $F_6S_{4.0}$ hydrogel and hydrogels loaded with fluorescein, rifampicin, erythromycin, and indomethacin (from left to right).

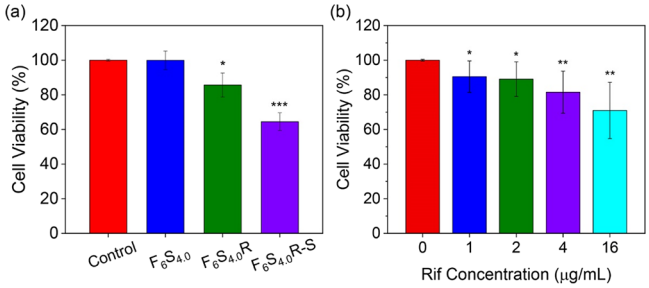

Figure 9. Viability of rabbit BMSCs after incubation in (a) extracts of $F_6S_{4.0}$ and $F_6S_{4.0}R$ hydrogels as well as in the extract solution after hydrogel stretching (denoted $F_6S_{4.0}R$-S) and (b) DMEM containing different concentrations of rifampicin for 36 h. * denotes statistically significant difference with $p < 0.05$ in comparison with the control group.

F127DA micelles at a concentration below 6 mmol/L, the mechanical properties of hydrogels increased with increasing concentration of macro-cross-linker because of the increment of hydrophobic association in the micelle cores. However, when the concentration of the macro-cross-linker was increased further, the high amount of hydrophobic micelle cores caused the phase separation of the hydrogel and resulted in the destruction of hydrogel homogeneity.[19] Microaggregates were observed on the cross sections of both $F_6S_{4.0}$ and $F_6S_{4.0}R$ hydrogels (Figure S10), which is probably due to the high solid content and phase separation in the micelle-cross-linked hydrogel.[36] In summary, incorporation of F127DA micelles as a macro-cross-linker with appropriate concentration could endow the hydrogel with outstanding strength and toughness because of the hydrophobic association (Scheme 1b,c).[37] In addition, it was observed that addition of hydrophobic rifampicin increased the mechanical properties of hydrogels significantly (Figure 1a), which may also be attributed to the enhancement of hydrophobic association in the macro-cross-linkers.

Several factors including polymer chain entanglement, electrostatic interactions of zwitterionic groups of polySBMA chains, and hydrophobic interactions of F127DA micelles contributed to the high toughness and resilience of the hydrogel. When the hydrogel was subjected to a certain mechanical force, polymer chains in the hydrogel network started to disentangle, followed by network orientation. The hydrophobic association of micelles was affected and even destroyed, causing deformation of micelles.[19] The hydrogen bonding and electrostatic interaction of polySBMA were also damaged under mechanical strain. Because of the reversible property of electrostatic interaction and hydrophobic association, the hydrogel recovered quickly after unloading.

3.3. Tissue Adhesion Property of F_xS_yR Hydrogels. Hydrogels with appropriate tissue adhesiveness offer favorable advantages over traditional dressings for wound treatments, such as ease of application and better compatibility with the skin during body movements. The adhesive strength of hydrogel to the porcine skin increased from 2.15 to 5.97 kPa with increasing polySBMA content in the hydrogel from 2 to 4 mol/L (Figure 2a). More interestingly, the hydrogel could adhere to the porcine skin repetitively, without significant decrease of the adhesion strength over at least six cycles (Figure 2b). This is because the SBMA monomeric unit in the hydrogel has a high dipole moment, which results in strong ion−dipole and dipole−dipole interactions with charged groups on the skin (e.g., carboxylic groups, amino groups, thiol groups, and so forth).[22] The result of adhesiveness means that a force of 0.48−1.34 N is required to remove the hydrogel with a size of 1.5 cm × 1.5 cm × 1 mm from the skin, which equals ∼200−600 times of the hydrogel's weight. Therefore, the hydrogel could adhere to the skin with good compatibility even with highly contoured surfaces, or during body movements. Moreover, compared to the adhesive strength, the tensile stress of the bulk hydrogel is much higher (11−112 kPa, Figure 1a). As a result, the hydrogel showed good compatibility with the skin surface and could be easily removed from the skin without any rupture or residue (Video S4).

3.4. Protein Adsorption Property. Protein adsorption on a material surface could lead to attachment of platelets, cells, and bacteria, which result in inflammation, granulation adhesion, and infection.[38] Severe protein adsorption may also impede antibiotic release from the hydrogel.[39,40] Compared with the clinically used chitin dressing and UrgoTul Ag dressing, protein adsorption on the $F_6S_{4.0}$ hydrogel was reduced by 35 and 8%, respectively (Figure 3). This is because zwitterionic polySBMA possesses high hydration ability to form a stable repulsive boundary layer under aqueous conditions.[41] In addition, as the hydrophobic cores of F127DA micelles were occupied by hydrophobic drugs, the hydrophobic interaction between the hydrogel and proteins is likely to be reduced,[42] resulting in a higher efficiency (>50%) in inhibiting protein adsorption compared to that of the $F_6S_{4.0}$ hydrogel.

3.5. Antibiofilm Property. Bacterial infection has been considered as one of the most challenging issues in wound treatment, which causes significant pain, fever, edema, and even severe complications.[43,44] UrgoClean is claimed to be bacteriostatic by entrapping bacterial cells in the dressing.[45] A large number of *S. aureus* cells (a common Gram-positive strain found in infected wounds) were observed on the fibers

https://dx.doi.org/10.1021/acsami.0c13009
ACS Appl. Mater. Interfaces 2020, 12, 52307−52318

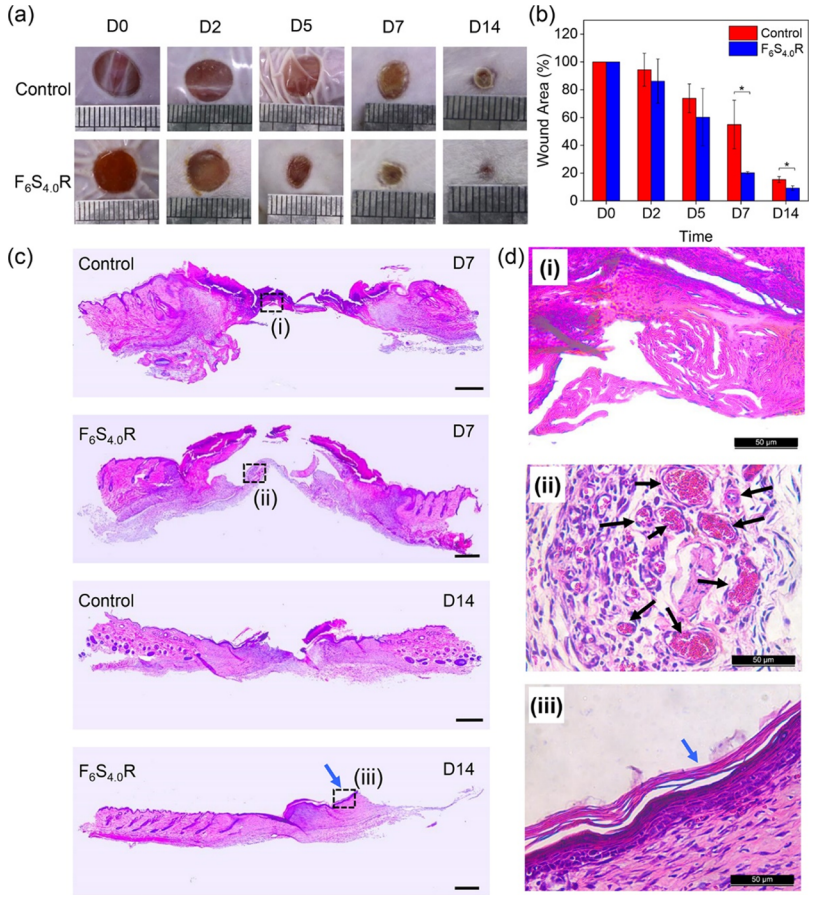

Figure 10. (a) Representative photos of wound beds, (b) wound size, and (c,d) H&E staining images of wound areas of the hydrogel group and the control group. Images in (d) show the corresponding area of (c) with a higher magnification. * denotes statistically significant difference with $p < 0.05$ in comparison with the control group. Scale bars in (c,d) represent 500 and 50 μm, respectively. Blue arrow: epithelium layer. Black arrow: blood vessels formed in the wound area.

of UrgoClean dressing (Figure 4a). However, less bacteria were observed on the surface of $F_6S_{4.0}$ hydrogel (Figure 4b). The remaining adherent bacteria appeared to be intact and in round shape (inset of Figure 4b), indicating that the $F_6S_{4.0}$ hydrogel has a limited bactericidal effect. On the other hand, few alive bacteria were observed on the surface of antibiotic-loaded $F_6S_{4.0}R$ hydrogel (Figure 4c), and the destroyed bacterial membrane can be clearly observed (inset of Figure 4c). Quantification analysis of biofilm formation showed that there were ~3.6×10^7 and ~1.2×10^7 bacterial cells/cm^2 on the surfaces of UrgoClean and UrgoTul Ag dressings, respectively (Figure 4d). *S. aureus* adhesion on the $F_6S_{4.0}$ hydrogel (without antibiotic) was reduced by ~2.33 orders of magnitude compared to that on UrgoClean. It has been widely reported that the hydrophilic zwitterionic polymer reduces bacterial adhesion by inhibiting the hydrophobic interaction between bacterial cells and the hydrogel surface.[46] With the addition of rifampicin to the hydrogel ($F_6S_{4.0}R$), the *S. aureus* biofilm on the surface was fully eliminated (Figure 4d). In addition, the $F_6S_{4.0}$ and $F_6S_{4.0}R$ hydrogels also showed excellent performance in inhibiting biofilm formation of *S. epidermidis* and *E. coli* (Figures 4e,f and S11), which are two other common pathogens found in wound infections. Compared to *S. aureus* and *S. epidermidis*, the $F_6S_{4.0}R$ hydrogel showed a relatively lower inhibiting efficacy against *E. coli* because of the higher MIC of rifampicin against *E. coli* (16 vs 0.008 and 0.063 μg/mL). In summary, the hydrogel showed excellent inhibitory efficacy on biofilm formation of both Gram-positive and Gram-negative bacteria.

3.6. Mechano-Responsive Drug Release from Hydrogel. Passive drug delivery is uncontrollable and unfavorable for the dynamic wound healing process. Because of the easy access and predictable control of mechanical stimuli compared to those of the conventional chemical and biological stimuli, application of mechano-responsive hydrogels is considered as an advanced and promising strategy for controlling drug delivery in a dynamic wound environment. In this study, drug delivery from a hydrogel under different mechanical conditions has been investigated. Approximately, 10% of encapsulated drugs was released passively from the $F_6S_{4.0}R$ hydrogel (exposed surface area: 21.6 cm^2) over 25 min without stretching (Figure 5a). While the hydrogel was stretched by 60%, which is close to the strain of human finger joints during bending, at a rate of 6 s/cycle for 250 cycles (i.e., 25 min), approximately 18% drugs were released from the $F_6S_{4.0}R$ hydrogel. The release ratio was further increased to 24% by increasing the tensile strain of the $F_6S_{4.0}R$ hydrogel to 80%. The cumulative drug release ratio was also enhanced by increasing the tensile cycles of the hydrogel (Figure 5a). For instance, when the tensile strain of the $F_6S_{4.0}R$ hydrogel was fixed at 80%, the cumulative drug release ratio was increased from 8% at 50 cycles to 24% at 250 cycles. In addition, it is reasonable to anticipate that by adjusting the amount of drugs in the hydrogel, the drug release rate could also be controlled.

https://dx.doi.org/10.1021/acsami.0c13009
ACS Appl. Mater. Interfaces 2020, 12, 52307−52318

Drug release from the $F_6S_{4.0}R$ hydrogel could also be enhanced by compressing the hydrogel (Figure 5b). It has been reported that the maximum in-shoe plantar pressure of human feet is ~120 kPa,[47] which is close to the pressure value on the $F_6S_{4.0}R$ hydrogel when it was compressed with a strain in the range of 40−60% (Figure 1d). When a compressive strain of 40% was applied to the hydrogel for 200 cycles, ~2.5% of drugs was released, which was significantly higher than the passive drug release of 1.1% from the hydrogel (exposed surface area: 0.94 cm^2) without compression over the same duration (20 min) (Figure 5b). The drug release ratio was further increased to 8.4 and 9.1% when the hydrogel was compressed by 50 and 60% for 200 cycles, respectively.

3.7. Drug Release Mechanism of Hydrogels. The above results clearly showed that a higher mechanical strain efficiently promoted drug release from the hydrogel matrix. To understand the drug release mechanism, the change in the nanostructure arrangement of hydrogels under tensile and compressive forces was analyzed using *in situ* SAXS (Figure 6). When the hydrogels were not subject to any mechanical strain, the SAXS scattering patterns of hydrogels with F127DA micelles ($F_6S_{4.0}$ and $F_6S_{4.0}R$) and without F127DA micelles ($S_{4.0}$) were all symmetrical and round, which indicates that polymer chains in the hydrogel network were randomly distributed. When it was stretched to 180% of its original length, the scattering pattern of $F_6S_{4.0}$ and $F_6S_{4.0}R$ hydrogels became elliptical, as a result of anisotropic scattering of the X-ray signals. A similar elliptical scattering pattern was also observed when $F_6S_{4.0}$ and $F_6S_{4.0}R$ hydrogels were compressed by 60% of their initial thickness. The micelles in the hydrogel, which serve as the energy dissipation unit, would first be deformed along the stretching or compressing direction,[48] resulting in aligned domains in the polymeric network (Figure S12). However, there was no obvious change in the scattering pattern of $S_{4.0}$ hydrogel (without F127DA micelles), regardless of whether it was stretched or compressed, indicating that the distribution of polymer chains in the hydrogel remained random (Figure S12). As illustrated in Scheme 1c, the micelles in the $F_6S_{4.0}R$ hydrogel network deform due to external mechanical force, resulting in the disruption of hydrophobic association in the micelle cores,[19,30,49] which caused the drug molecule in the hydrophobic core to destabilize and release into the hydrogel matrix. Because of the porous structure and high water content of hydrogels, drugs finally diffused into the external aqueous environment.[50,51] In this way, a sustainable and mechano-responsive release of drugs from hydrogels was achieved.

3.8. *In Vitro* Antibacterial Assay. The disk diffusion method was used to evaluate the hydrogel's capability to inhibit bacterial growth. Figure 7a demonstrates the antibacterial properties of $F_6S_{4.0}R$ hydrogel against *S. aureus* under different tensile strains compared with those of the control group (PBS solution). Higher antibacterial capability of the solution with drugs released from hydrogels with stretching was observed compared to the group from hydrogels without stretching. By increasing the tensile strain from 60 to 80%, more drug was released from the hydrogel, and a larger inhibitory zone was observed. A similar increasing trend of antibacterial effect was observed as the compressive strain of hydrogel was increased from 40 to 60% (Figure 7b). The inhibitory zone diameter increased with the increase of the stretching cycles at a fixed tensile strain because more amount of antibiotics was released from the hydrogel with continuous stretching, and the released drug showed a broad-spectrum antibacterial property against Gram-positive *S. aureus* and *S. epidermidis* and Gram-negative *E. coli* (Figure S13).

3.9. *Ex Vivo* Drug Penetration Evaluation. Spatial penetration of therapeutic drugs such as antibiotics, pain killers, and anti-inflammatory drugs into the skin tissue is essential in the wound healing process. To simulate drug penetration from the hydrogel into the wounded skin tissue, an *ex vivo* drug penetration test was conducted. In order to mimic a full-thickness skin defect, the porcine tissue with epidermis and dermis removed was used in the test. Hydrophobic fluorescein, *N*-butyl-4-(2-aminoethylamino)-1,8-naphthalimide, was encapsulated in the hydrogel as a probe molecule to characterize the penetration process from the hydrogel through the skin tissue. The confocal fluorescence images of the section of porcine tissue without and with the compression process of the hydrogel−tissue assembly are shown in Figure 8a,b, respectively. It was observed that the penetration depth of the hydrophobic fluorescein released from the hydrogel after 60% compressive strain for 1000 cycles was greater than that of samples without compression. After compression, the penetration depth of fluorescein was more than 1200 μm, as measured by image analysis (Figure 8c). However, for samples without compression, the depth of fluorescein by passive diffusion over the same duration (100 min) was approximately 500 μm. In addition, the disk diffusion test confirmed that rifampicin could penetrate through the pig tissue of 3 mm in thickness and collected in a filter paper after cyclic compression (Figure S14). The above results showed that mechanical stress can not only enhance drug release but also promote drug penetration into tissues. The hydrogel could be used as a universal platform for the encapsulation of different hydrophobic bioactive drugs (e.g., rifampicin, erythromycin, and indomethacin, Figure 8d). This property of mechano-responsive hydrogels is promising for treatment of acute wounds in a complicated dynamic environment.

3.10. Biocompatibility Evaluation. Biocompatibility is essential for successful wound dressing applications. The cytotoxicity assay of hydrogels was conducted using rabbit BMSCs according to the standard protocol stated in ISO 10993-5:2009.[28] The $F_6S_{4.0}$ hydrogel showed minimal cytotoxicity with a cell viability of ≥99% after incubation in the $F_6S_{4.0}$ extract for 36 h (Figure 9a). The cell viability with the extract of rifampicin-loaded $F_6S_{4.0}R$ hydrogel (extract containing 5.13 μg/mL rifampicin) was slightly decreased to 85%. The cell viability with an extract in which the $F_6S_{4.0}R$ hydrogel was stretched by 80% for 250 cycles (with identical experimental conditions to the antibacterial test, containing 13.70 μg/mL rifampicin) was about 64%. It showed a mild inhibitory effect of rifampicin on the cells,[52] as the cell viability slightly decreased with increasing concentration of rifampicin in the culture medium (Figure 9b). Overall, the micelle-cross-linked zwitterionic hydrogel showed low toxicity to mammalian cells and is expected to be applicable for wound dressings.

3.11. *In Vivo* Skin Irritation and Wound Healing Performance. The irritation test was conducted to evaluate skin compatibility of the hydrogel. No erythema, eschar, or edema formation was observed on the skins in the $F_6S_{4.0}R$ hydrogel group and the control group (gauze with PBS). The H&E staining image demonstrated that the epidermis was intact and no inflammation infiltration was observed (Figure S15). The irritant response of the hydrogel to the mouse skin was negligible according to the irritation score (Table S2). To

https://dx.doi.org/10.1021/acsami.0c13009
ACS Appl. Mater. Interfaces 2020, 12, 52307−52318

evaluate the *in vivo* performance of $F_6S_{4.0}R$ hydrogel on wound healing, a full-thickness skin defect mice model was used. The wound size of the hydrogel group became smaller than that of the control group from day 2 onward (Figure 10a), and it significantly decreased by 63.2 and 40.2% compared to that of control on day 7 and day 14, respectively (Figure 10b). H&E staining images demonstrated that on day 7, formation of new blood vessels (indicated by black arrows in Figure 10d) was observed in the wound area treated with hydrogel. There were fewer inflammatory cell nuclei (dyed blue) around the wound bed in the $F_6S_{4.0}R$ group (Figure 10c), indicating that less inflammatory infiltration was found in the $F_6S_{4.0}R$ group, probably due to enhanced healing capacity of the hydrogel. On day 14, an epithelium layer on the wound site was formed in the $F_6S_{4.0}R$ group, and the regenerated structure could be clearly observed (Figure 10d), whereas the wound was not fully closed in the control group. It should be noted that because the polySBMA network is hard to be degraded, the $F_6S_{4.0}R$ hydrogel was stable under both *in vitro* and *in vivo* conditions. Only a slight weight loss (approximately 7.5%) was observed after the hydrogel was incubated in PBS for >10 days, and the hydrogel maintained its original structure on the mouse skin wound for at least 5 days (Figure S16). As a result, the hydrogel could support wound healing over a prolonged period. In summary, treatment of wounds with the $F_6S_{4.0}R$ hydrogel exhibited an enhanced healing performance.

4. CONCLUSIONS

In summary, a tough antibacterial and antifouling hydrogel with mechano-responsive delivery of drugs has been developed in this study. The zwitterionic hydrogel prevented protein adsorption and bacterial adhesion, attributed to the excellent antifouling properties of hydrophilic polySBMA. The drug-loaded micelles in the hydrogel deformed subjected to mechanical stresses, resulting in a reduction of hydrophobic interactions between the drug and the micelle core and enhancement of drug release. Therefore, a mechano-responsive release profile of drugs from the hydrogel was achieved. In addition, drug penetration from the hydrogel into porcine tissues was enhanced under mechanical stress. The hydrogel exhibited a broad-spectrum antibacterial property against Gram-positive and Gram-negative bacteria and showed good biocompatibility with mammalian cells. The hydrogel showed negligible irritation to skin and could promote wound healing in a mouse model. Such a tough mechano-responsive antibacterial hydrogel holds great promise for treatment of wounds in a dynamic mechanical environment.

■ ASSOCIATED CONTENT

Supporting Information

The Supporting Information is available free of charge at https://pubs.acs.org/doi/10.1021/acsami.0c13009.

Chemical compositions used in the hydrogel preparation in this study; schematic illustration of the hydrogel−porcine skin assembly used in the lap shear test; schematic illustration of the device used in drug release tests upon hydrogel stretching and compression; schematic illustration of assembly used for drug penetration by hydrogel compression; chemical structure and ^{1}H NMR spectrum of F127DA; DLS results of F127DA, rifampicin, and rifampicin-loaded F127DA; loading efficiency of rifampicin in F127DA micelles; fracture strength, fracture strain, and tensile modulus of prepared hydrogels; swelling ratio of $F_6S_{4.0}$ hydrogels in different concentrations of NaCl; tensile stress−strain curves of hydrogels prepared with different contents of NaCl and F127DA; SEM images of cross-sectional morphology of prepared hydrogels; SEM images of *E. coli* biofilm formation; an illustration of the change in hydrogel network before and after mechanical loading; inhibitory zone diameter of different drug release solutions; images of the inhibitory zone of penetrated rifampicin against *S. aureus*; skin irritation test of the $F_6S_{4.0}R$ hydrogel; and degradability of the $F_6S_{4.0}R$ hydrogel (PDF)

Drug release upon hydrogel stretching (MP4)

Drug release upon hydrogel compression (MP4)

Ex vivo drug penetration test (MP4)

Hydrogel adhesion (MP4)

■ AUTHOR INFORMATION

Corresponding Authors

Rong Wang − *Cixi Institute of Biomedical Engineering, Ningbo Institute of Materials Technology and Engineering, Chinese Academy of Sciences, Ningbo 315300, China;* orcid.org/0000-0003-1971-0865; Email: rong.wang@nimte.ac.cn

Donglei Liu − *School of Mechatronics Engineering, Nanchang University, Nanchang 330031, China*; Email: dlliu@ncu.edu.cn

Jun Fu − *School of Materials Science and Engineering, Sun Yat-sen University, Guangzhou 510275, China;* orcid.org/0000-0002-8723-1439; Email: fujun8@mail.sysu.edu.cn

Authors

Kun Fang − *School of Mechatronics Engineering, Nanchang University, Nanchang 330031, China; Cixi Institute of Biomedical Engineering, Ningbo Institute of Materials Technology and Engineering, Chinese Academy of Sciences, Ningbo 315300, China*

Hua Zhang − *Cixi Institute of Biomedical Engineering, Ningbo Institute of Materials Technology and Engineering, Chinese Academy of Sciences, Ningbo 315300, China*

Linjie Zhou − *Cixi Institute of Biomedical Engineering, Ningbo Institute of Materials Technology and Engineering, Chinese Academy of Sciences, Ningbo 315300, China*

Ting Xu − *Cixi Institute of Biomedical Engineering, Ningbo Institute of Materials Technology and Engineering, Chinese Academy of Sciences, Ningbo 315300, China*

Ying Xiao − *Cixi Institute of Biomedical Engineering, Ningbo Institute of Materials Technology and Engineering, Chinese Academy of Sciences, Ningbo 315300, China*

Yang Zhou − *Cixi Institute of Biomedical Engineering, Ningbo Institute of Materials Technology and Engineering, Chinese Academy of Sciences, Ningbo 315300, China*

Guorong Gao − *Cixi Institute of Biomedical Engineering, Ningbo Institute of Materials Technology and Engineering, Chinese Academy of Sciences, Ningbo 315300, China*

Jing Chen − *Cixi Institute of Biomedical Engineering, Ningbo Institute of Materials Technology and Engineering, Chinese Academy of Sciences, Ningbo 315300, China;* orcid.org/0000-0002-0024-4561

Fanrong Ai − *School of Mechatronics Engineering, Nanchang University, Nanchang 330031, China*

https://dx.doi.org/10.1021/acsami.0c13009
ACS Appl. Mater. Interfaces 2020, 12, 52307−52318

Complete contact information is available at:
https://pubs.acs.org/10.1021/acsami.0c13009

Author Contributions

The manuscript was written through contributions of all authors. All authors have given approval to the final version of the manuscript.

Notes

The authors declare no competing financial interest.

■ ACKNOWLEDGMENTS

This work was funded by the National Natural Science Foundation of China (51803229, 51873224, and 52011530019), National Key Research and Development Program of China (2018YFE0119400), S&T Innovation 2025 Major Special Program of Ningbo (2018B10040), and Natural Science Foundation of Zhejiang Province (LQ19E030006).

■ REFERENCES

(1) Qu, J.; Zhao, X.; Liang, Y.; Zhang, T.; Ma, P. X.; Guo, B. Antibacterial Adhesive Injectable Hydrogels with Rapid Self-Healing, Extensibility and Compressibility as Wound Dressing for Joints Skin Wound Healing. *Biomaterials* **2018**, *183*, 185−199.
(2) Wang, C.; Wang, M.; Xu, T.; Zhang, X.; Lin, C.; Gao, W.; Xu, H.; Lei, B.; Mao, C. Engineering Bioactive Self-Healing Antibacterial Exosomes Hydrogel for Promoting Chronic Diabetic Wound Healing and Complete Skin Regeneration. *Theranostics* **2019**, *9*, 65−76.
(3) Chen, G.; Yu, Y.; Wu, X.; Wang, G.; Ren, J.; Zhao, Y. Bioinspired Multifunctional Hybrid Hydrogel Promotes Wound Healing. *Adv. Funct. Mater.* **2018**, *28*, 1801386.
(4) Lin, Y.-J.; Lee, G.-H.; Chou, C.-W.; Chen, Y.-P.; Wu, T.-H.; Lin, H.-R. Stimulation of Wound Healing by PU/Hydrogel Composites Containing Fibroblast Growth Factor-2. *J. Mater. Chem. B* **2015**, *3*, 1931−1941.
(5) Xie, C.; Li, P.; Han, L.; Wang, Z.; Zhou, T.; Deng, W.; Wang, K.; Lu, X. Electroresponsive and Cell-Affinitive Polydopamine/Polypyrrole Composite Microcapsules with A Dual-Function of On-Demand Drug Delivery and Cell Stimulation for Electrical Therapy. *NPG Asia Mater.* **2017**, *9*, No. e358.
(6) Wang, R.; Li, J.; Chen, W.; Xu, T.; Yun, S.; Xu, Z.; Xu, Z.; Sato, T.; Chi, B.; Xu, H. A Biomimetic Mussel-Inspired ε-Poly-L-lysine Hydrogel with Robust Tissue-Anchor and Anti-Infection Capacity. *Adv. Funct. Mater.* **2017**, *27*, 1604894.
(7) Li, S.; Dong, S.; Xu, W.; Tu, S.; Yan, L.; Zhao, C.; Ding, J.; Chen, X. Antibacterial Hydrogels. *Adv. Sci.* **2018**, *5*, 1700527.
(8) Ballance, W. C.; Seo, Y.; Baek, K.; Chalifoux, M.; Kim, D.; Kong, H. Stretchable, Anti-Bacterial Hydrogel Activated by Large Mechanical Deformation. *J. Controlled Release* **2018**, *275*, 1−11.
(9) Di, J.; Yao, S.; Ye, Y.; Cui, Z.; Yu, J.; Ghosh, T. K.; Zhu, Y.; Gu, Z. Stretch-Triggered Drug Delivery from Wearable Elastomer Films Containing Therapeutic Depots. *ACS Nano* **2015**, *9*, 9407−9415.
(10) Chen, J.; Peng, Q.; Peng, X.; Han, L.; Wang, X.; Wang, J.; Zeng, H. Recent Advances in Mechano-Responsive Hydrogels for Biomedical Applications. *ACS Appl. Polym. Mater.* **2020**, *2*, 1092−1107.
(11) Wang, J.; Kaplan, J. A.; Colson, Y. L.; Grinstaff, M. W. Mechanoresponsive Materials for Drug Delivery: Harnessing Forces for Controlled Release. *Adv. Drug Delivery Rev.* **2017**, *108*, 68−82.
(12) Kataoka, K.; Harada, A.; Nagasaki, Y. Block Copolymer Micelles for Drug Delivery: Design, Characterization and Biological Significance. *Adv. Drug Delivery Rev.* **2012**, *64*, 37−48.
(13) Kwon, G. S.; Kataoka, K. Block Copolymer Micelles as Long-Circulating Drug Vehicles. *Adv. Drug Delivery Rev.* **1995**, *16*, 295−309.
(14) Cabral, H.; Miyata, K.; Osada, K.; Kataoka, K. Block Copolymer Micelles in Nanomedicine Applications. *Chem. Rev.* **2018**, *118*, 6844−6892.
(15) Wang, R.; Chua, K. L.; Neoh, K. G. Bifunctional Coating with Sustained Release of 4-Amide-Piperidine-C12 for Long-Term Prevention of Bacterial Colonization on Silicone. *ACS Biomater. Sci. Eng.* **2015**, *1*, 405−415.
(16) Li, Y.; Sun, Y.; Xiao, Y.; Gao, G.; Liu, S.; Zhang, J.; Fu, J. Electric Field Actuation of Tough Electroactive Hydrogels Cross-Linked by Functional Triblock Copolymer Micelles. *ACS Appl. Mater. Interfaces* **2016**, *8*, 26326−26331.
(17) Yu, X.; Qin, Z.; Wu, H.; Lv, H.; Yang, X. Tuning Hydrogel Mechanics by Kinetically Dependent Cross-Linking. *Macromolecules* **2019**, *52*, 1249−1256.
(18) Li, Y.; Yang, C.; Khan, M.; Liu, S.; Hedrick, J. L.; Yang, Y.-Y.; Ee, P.-L. R. Nanostructured PEG-Based Hydrogels with Tunable Physical Properties for Gene Delivery to Human Mesenchymal Stem Cells. *Biomaterials* **2012**, *33*, 6533−6541.
(19) Xu, Z.; Li, J.; Gao, G.; Wang, Z.; Cong, Y.; Chen, J.; Yin, J.; Nie, L.; Fu, J. Tough and Self-Recoverable Hydrogels Crosslinked by Triblock Copolymer Micelles and Fe^{3+} Coordination. *J. Polym. Sci., Part B: Polym. Phys.* **2018**, *56*, 865−876.
(20) Ladd, J.; Zhang, Z.; Chen, S.; Hower, J. C.; Jiang, S. Zwitterionic Polymers Exhibiting High Resistance to Nonspecific Protein Adsorption from Human Serum and Plasma. *Biomacromolecules* **2008**, *9*, 1357−1361.
(21) Lalani, R.; Liu, L. Electrospun Zwitterionic Poly(Sulfobetaine Methacrylate) for Nonadherent, Superabsorbent, and Antimicrobial Wound Dressing Applications. *Biomacromolecules* **2012**, *13*, 1853−1863.
(22) Wang, L.; Gao, G.; Zhou, Y.; Xu, T.; Chen, J.; Wang, R.; Zhang, R.; Fu, J. Tough, Adhesive, Self-Healable, and Transparent Ionically Conductive Zwitterionic Nanocomposite Hydrogels as Skin Strain Sensors. *ACS Appl. Mater. Interfaces* **2019**, *11*, 3506−3515.
(23) Zhu, Y.; Zhang, J.; Yang, J.; Pan, C.; Xu, T.; Zhang, L. Zwitterionic Hydrogels Promote Skin Wound Healing. *J. Mater. Chem. B* **2016**, *4*, 5105−5111.
(24) Zhang, L.; Cao, Z.; Bai, T.; Carr, L.; Ella-Menye, J.-R.; Irvin, C.; Ratner, B. D.; Jiang, S. Zwitterionic Hydrogels Implanted in Mice Resist the Foreign-body Reaction. *Nat. Biotechnol.* **2013**, *31*, 553−556.
(25) Sun, Y.-n.; Gao, G.-r.; Du, G.-l.; Cheng, Y.-j.; Fu, J. Super Tough, Ultrastretchable, and Thermoresponsive Hydrogels with Functionalized Triblock Copolymer Micelles as Macro-Cross-Linkers. *ACS Macro Lett.* **2014**, *3*, 496−500.
(26) Tilinca, M.; Hancu, G.; Mircia, E.; Iriminescu, D.; Rusu, A.; Vlad, A. R.; Barabás, E. Simultaneous Determination of Isoniazid and Rifampicin by UV Spectrophotometry. *Farmacia* **2017**, *65*, 219−224.
(27) Bradford, M. M. A Rapid and Sensitive Method for the Quantitation of Microgram Quantities of Protein Utilizing The Principle of Protein-Dye Binding. *Anal. Biochem.* **1976**, *72*, 248−254.
(28) ISO 10993-5:2009. *Biological Evaluation of Medical Devices—Part 5: Tests for In Vitro Cytotoxicity*, 2009.
(29) ISO 10993-10:2010. *Biological Evaluation of Medical Devices—Part 10: Tests for Irritation and Skin Sensitization*, 2010.
(30) Xu, D.; Xu, T.; Gao, G.; Xiao, Y.; Wang, Z.; Chen, J.; Zhou, Y.; Wang, R.; Yin, J.; Fu, J. Effect of Solvent-Matrix Interactions on Structures and Mechanical Properties of Micelle-Crosslinked Gels. *J. Polym. Sci., Part B: Polym. Phys.* **2019**, *57*, 473−483.
(31) Di Biase, M.; de Leonardis, P.; Castelletto, V.; Hamley, I. W.; Derby, B.; Tirelli, N. Photopolymerization of Pluronic F127 Diacrylate: A Colloid-Templated Polymerization. *Soft Matter* **2011**, *7*, 4928−4937.
(32) Cabral, H.; Kataoka, K. Progress of Drug-Loaded Polymeric Micelles into Clinical Studies. *J. Controlled Release* **2014**, *190*, 465−476.
(33) Eshel-Green, T.; Bianco-Peled, H. Mucoadhesive Acrylated Block Copolymers Micelles for The Delivery of Hydrophobic Drugs. *Colloids Surf., B* **2016**, *139*, 42−51.

(34) Liu, J.; Zheng, H.; Poh, P.; Machens, H.-G.; Schilling, A. Hydrogels for Engineering of Perfusable Vascular Networks. *Int. J. Mol. Sci.* **2015**, *16*, 15997−16016.
(35) Yang, B.; Wang, C.; Zhang, Y.; Ye, L.; Qian, Y.; Shu, Y.; Wang, J.; Li, J.; Yao, F. A Thermoresponsive Poly(*N*-Vinylcaprolactam-*co*-Sulfobetaine Methacrylate) Zwitterionic Hydrogel Exhibiting Switchable Anti-Biofouling and Cytocompatibility. *Polym. Chem.* **2015**, *6*, 3431−3442.
(36) Kim, H.-J.; Cho, S.; Oh, S. J.; Shin, S. G.; Ryu, H. W.; Jeong, J. H. Tuning the Hydrophobicity of a Hydrogel Using Self-Assembled Domains of Polymer Cross-Linkers. *Materials* **2019**, *12*, 1635.
(37) Ghoorchian, A.; Simon, J. R.; Bharti, B.; Han, W.; Zhao, X.; Chilkoti, A.; López, G. P. Bioinspired Reversibly Cross-Linked Hydrogels Comprising Polypeptide Micelles Exhibit Enhanced Mechanical Properties. *Adv. Funct. Mater.* **2015**, *25*, 3122−3130.
(38) Chen, H.; Chen, Q.; Hu, R.; Wang, H.; Newby, B.-m. Z.; Chang, Y.; Zheng, J. Mechanically Strong Hybrid Double Network Hydrogels with Antifouling Properties. *J. Mater. Chem. B* **2015**, *3*, 5426−5435.
(39) Liu, S. Q.; Yang, C.; Huang, Y.; Ding, X.; Li, Y.; Fan, W. M.; Hedrick, J. L.; Yang, Y.-Y. Antimicrobial and Antifouling Hydrogels Formed In Situ from Polycarbonate and Poly(Ethylene Glycol) via Michael Addition. *Adv. Mater.* **2012**, *24*, 6484−6489.
(40) GhavamiNejad, A.; Park, C. H.; Kim, C. S. In Situ Synthesis of Antimicrobial Silver Nanoparticles within Antifouling Zwitterionic Hydrogels by Catecholic Redox Chemistry for Wound Healing Application. *Biomacromolecules* **2016**, *17*, 1213−1223.
(41) Zhu, Y.; Wang, J.; Zhang, F.; Gao, S.; Wang, A.; Fang, W.; Jin, J. Zwitterionic Nanohydrogel Grafted PVDF Membranes with Comprehensive Antifouling Property and Superior Cycle Stability for Oil-In-Water Emulsion Separation. *Adv. Funct. Mater.* **2018**, *28*, 1804121.
(42) Neacsu, M. V.; Matei, I.; Micutz, M.; Staicu, T.; Precupas, A.; Popa, V. T.; Salifoglou, A.; Ionita, G. Interaction Between Albumin and Pluronic F127 Block Copolymer Revealed by Global and Local Physicochemical Profiling. *J. Phys. Chem. B* **2016**, *120*, 4258−4267.
(43) Percival, S. L.; McCarty, S. M.; Lipsky, B. Biofilms and Wounds: An Overview of The Evidence. *Adv. Wound Care* **2015**, *4*, 373−381.
(44) Hurlow, J.; Couch, K.; Laforet, K.; Bolton, L.; Metcalf, D.; Bowler, P. Clinical Biofilms: A Challenging Frontier in Wound Care. *Adv. Wound Care* **2015**, *4*, 295−301.
(45) UrgoMedical Homepage. http://www.urgomedical.com/products/urgoclean/ (retrieved July 2020).
(46) Mi, L.; Jiang, S. Integrated Antimicrobial and Nonfouling Zwitterionic Polymers. *Angew. Chem., Int. Ed.* **2014**, *53*, 1746−1754.
(47) Wafai, L.; Zayegh, A.; Woulfe, J.; Aziz, S.; Begg, R. Identification of Foot Pathologies Based on Plantar Pressure Asymmetry. *Sensors* **2015**, *15*, 20392−20408.
(48) Xiao, L.; Zhu, J.; Londono, J. D.; Pochan, D. J.; Jia, X. Mechano-Responsive Hydrogels Crosslinked by Block Copolymer Micelles. *Soft Matter* **2012**, *8*, 10233−10237.
(49) Ma, J.; Lee, J.; Han, S. S.; Oh, K. H.; Nam, K. T.; Sun, J.-Y. Highly Stretchable and Notch-Insensitive Hydrogel Based on Polyacrylamide and Milk Protein. *ACS Appl. Mater. Interfaces* **2016**, *8*, 29220−29226.
(50) Slaughter, B. V.; Khurshid, S. S.; Fisher, O. Z.; Khademhosseini, A.; Peppas, N. A. Hydrogels in Regenerative Medicine. *Adv. Mater.* **2009**, *21*, 3307−3329.
(51) Wei, L.; Cai, C.; Lin, J.; Chen, T. Dual-Drug Delivery System Based on Hydrogel/Micelle Composites. *Biomaterials* **2009**, *30*, 2606−2613.
(52) Blanchemain, N.; Laurent, T.; Chai, F.; Neut, C.; Haulon, S.; Krump-konvalinkova, V.; Morcellet, M.; Martel, B.; Kirkpatrick, C. J.; Hildebrand, H. F. Polyester Vascular Prostheses Coated with A Cyclodextrin Polymer and Activated with Antibiotics: Cytotoxicity and Microbiological Evaluation. *Acta Biomater.* **2008**, *4*, 1725−1733.

https://dx.doi.org/10.1021/acsami.0c13009
ACS Appl. Mater. Interfaces 2020, 12, 52307−52318